Available online at www.sciencedirect.com
SCIENCE DIRECT
Journal of Power Sources 158 (2006) 1–12
JOURNAL OF POWER SOURCES
www.elsevier.com/locate/jpowsour

Strategic enzyme patterning for microfluidic biofuel cells

E. Kjeang [a], D. Sinton [a,*], D.A. Harrington [b]

[a] *Department of Mechanical Engineering, Institute for Integrated Energy Systems (IESVic), University of Victoria, P.O. Box 3055 STN CSC, Vic., BC, Canada V8W 3P6*
[b] *Department of Chemistry, Institute for Integrated Energy Systems (IESVic), University of Victoria, P.O. Box 3055 STN CSC, Vic., BC, Canada V8W 3P6*

Received 12 July 2005; accepted 30 July 2005
Available online 1 December 2005

Abstract

The specific character of biological enzyme catalysts enables combined fuel and oxidant channels and simplified non-compartmentalized fuel cell assemblies. In this work, a microstructured enzymatic biofuel cell architecture is proposed, and species transport phenomena combined with consecutive chemical reactions are studied computationally in order to provide guidelines for optimization. This is the first computational study of this technology, and a 2D CFD model for species transport coupled with laminar fluid flow and Michaelis–Menten enzyme kinetics is established. It is shown that the system is reaction rate limited, indicating that enzyme specific turnover numbers are key parameters for biofuel cell performance. Separated and mixed enzyme patterns in different proportions are analyzed for various Peclet numbers. High fuel utilization is achieved in the diffusion dominated and mixed species transport regimes with separated enzymes arranged in relation to individual turnover rates. However, the Peclet number has to be above a certain threshold value to obtain satisfying current densities. The mixed transport regime is particularly attractive while current densities are maintained close to maximum levels. Optimum performance is achieved by mixed enzyme patterning tailored with respect to individual turnover rates, enabling high current densities combined with nearly complete fuel utilization.

Keywords: Biofuel cell; Enzyme kinetics; Biocatalysis; Microfluidics; Numerical modeling; Consecutive reactions

1. Introduction

In recent years, the demand on the power supplies of portable electronic equipment such as laptops and cellular phones has substantially increased due to additional technical features and miniaturization efforts. Well-developed lithium ion battery technology currently powers most of these applications. It is unlikely, however, that improvements in battery technology will keep pace with the accelerating power demand [1]. In order to enable further advances, other alternatives such as fuel cells have to be considered. The high cost associated with the development of new small-scale fuel cell power supplies are surpassed by the growing portable power needs of the mobile workforce and the major industries that now support them [2]. Direct methanol fuel cells exhibit relatively high power and energy densities [3], but there are several problems associated with these, for instance methanol crossover and slow anode kinetics reduce efficiency and open-circuit voltage [4-5]. Recently, this technology has been challenged by emerging microscale biofuel cell designs.

A biofuel cell is not necessarily a fuel cell that uses a biological fuel, although that might very well be the case. Biofuel cells always involve biological molecules or living cells to catalyze the chemical reactions, replacing conventional transition metal catalysts such as platinum. The underlying concept is to control electrochemical processes occurring in nature to provide useful electrical current. Chemical energy can be converted to electrical energy by coupling the biocatalytic oxidation of organic or inorganic compounds to the chemical reduction of an oxidant in a controlled environment. There are two main types of biofuel cells; microbial biofuel cells and enzymatic biofuel cells. Microbial fuel cells utilize entire living cells or microorganisms combined with redox intermediates to catalyze the oxidation of a fuel. Microbe catalyzed processes involve several fairly complex steps with various intermediates [6] and are quite inefficient [7]. In an enzymatic biofuel cell, the chemical reactions are catalyzed by biological redox enzymes that can be separated and

* Corresponding author. Tel.: +1 250 721 8623; fax: +1 250 721 6051.
E-mail address: dsinton@me.uvic.ca (D. Sinton).

0378-7753/$ – see front matter © 2005 Elsevier B.V. All rights reserved.
doi:10.1016/j.jpowsour.2005.07.092

Nomenclature

A_c	cross-sectional area (m^2)
c	concentration ($mol\,m^{-3}$)
D	solute diffusivity ($m^2\,s^{-1}$)
D_h	hydraulic diameter (m)
Da	Damköhler number
F	Faraday's constant ($C\,mol^{-1}$)
FU	fuel utilization
g	constant of gravity ($m\,s^{-2}$)
h	channel height (m)
i	current density ($A\,m^{-2}$)
J	species molar flux ($mol\,s^{-1}\,m^{-2}$)
k	rate constant (s^{-1})
k_{cat}	turnover number (s^{-1})
K_m	sensitivity ($mol\,m^{-3}$)
L	axial length of electrode (m)
L_c	characteristic length (m)
M	molar mass ($kg\,mol^{-1}$)
N_A	Avogadro's number (mol^{-1})
p	pressure (Pa)
Pe	Peclet number
R	turnover rate ($mol\,s^{-1}\,m^{-2}$)
Re	Reynolds number
t	time (s)
T	temperature (K)
u	bulk velocity ($m\,s^{-1}$)
$\bar{u}$	mean bulk velocity ($m\,s^{-1}$)
V_{out}	output voltage (V)
$\dot{V}$	volumetric flow rate ($m^3\,s^{-1}$)
v	specific activity ($mol\,kg^{-1}\,s^{-1}$)
w	channel width (m)
$\dot{W}_{out}$	output power (W)
$\dot{W}_p$	pumping power (W)
x	direction of main flow (axial)
y	direction across channel (transverse)
z	number of electrons

Greek letters

μ	kinematic viscosity ($kg\,m^{-1}s^{-1}$)
ρ	density ($kg\,m^{-3}$)

Subscripts

in	inlet value
max	maximum value
out	outlet value
ref	reference value
0	bulk value

Superscripts

A	methanol dehydrogenase (MDH)
ADH	alcohol dehydrogenase
B	formaldehyde dehydrogenase (FalDH)
C	formate dehydrogenase (FDH)

purified from suitable organisms, thus extracting the actual part of the cell that enables catalytic operation [8]. Enzyme catalysts are specific to particular substances (fuels) and the presence of other substances does not, in general, impact the rate of catalysis. This specificity of enzyme catalysis enables the combination of fuel and oxidant streams in a single manifold [8], with multiple benefits in the context of fuel cell design and operation: no proton exchange membrane is needed, sealing, manifolding and fluid delivery requirements are greatly reduced, ohmic losses and water management issues associated with proton exchange membrane fuel cell (PEMFC) technologies are eliminated [9], as are two-phase transport issues associated with gas diffusion layers [10]. With fuel and oxidant streams fully mixed in the same channel, fuel crossover is also not a problem. Cost reduction is possibly the main aspect that can make biological fuel cells competitive for small-scale power supplies. Firstly, the proton exchange membrane is a costly component of conventional fuel cell assemblies [11]. Secondly, the cost of platinum, which is already high, is expected to increase further with increased demand and production [12]. Biological enzymes, on the other hand, are derived from naturally abundant organisms and can be produced using low-cost fermentation techniques [13]. Other benefits are operation near or at room temperature and compact units produced by inexpensive and well-established microfabrication methods. Channels down to 10 μm in diameter can be fabricated, greatly improving the active surface-to-volume ratio of the device and consequently its power density, which remains quite limited with current biofuel cell designs. As with all fuel cell technologies, however, stability is a key issue for biofuel cells [13]. Enzymatic biofuel cells must withstand extended use, varied duty cycles, a range of environmental conditions and must reach lifetimes satisfying the demands of advanced applications, preferably on the order of years. Possible applications range from miniaturized portable electronic equipment [2] and sensors to integrated lab-on-chip power supplies [14] and advanced in vivo diagnostic medical devices with reactants available in the ambient environment [13].

In most enzymatic biofuel cells developed to date, enzymes are placed in solution and the electron transfer from the enzyme biocatalysts to the electrode is mediated by a redox couple. The rate of electron transfer is generally limited by the ability of the redox species to diffuse back and forth. Several methods to improve electron transfer rates by immobilization of enzymes on electrode surfaces have been presented, for example: covalent enzyme–electrode polymer linkages, layered electrodes obtained by functional monolayers and non-covalent coupling by hydrophobic/hydrophillic or affinity interactions [15]. Electron mediators (co-factors) extracting electrons from the active sites of the enzymes are necessary for efficient flow of electrical current [8]. Alcohol dehydrogenase enzymes were immobilized in Nafion by Moore et al. [14] and their ethanol fuelled anode reached an open-circuit voltage of 0.34 V and current densities of 53 $\mu A\,cm^{-2}$ using an external platinum cathode. The highest open-circuit voltage (0.71 V) and power density ($1.5\,mW\,cm^{-2}$) for a methanol/oxygen biofuel cell was observed when the biocatalyst was immobilized close to the anode and utilized its electron mediator [16]. To achieve this, complete oxidation of

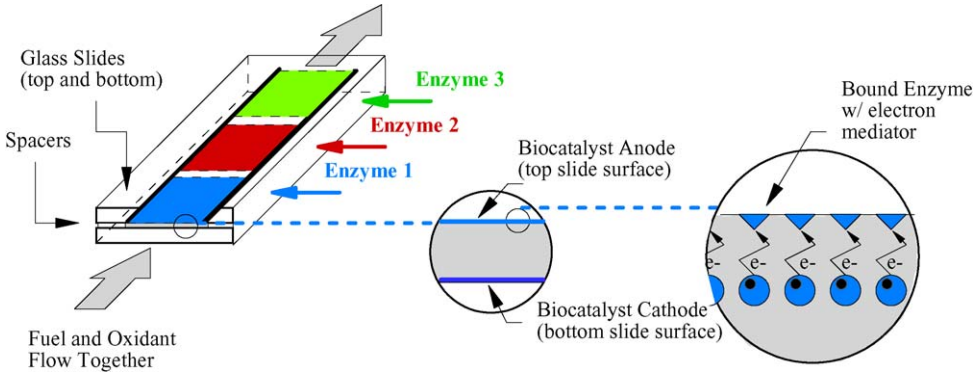

Fig. 1. Proof-of-concept microfluidic biofuel cell design.

methanol to carbon dioxide by three different enzymes was engaged. Patterning multiple enzyme electrodes to harness consecutive reactions represents a significant opportunity for biofuel cell technologies, particularly with respect to fuel utilization.

The biocatalysts of interest here are covalently linked directly to the electrode surface via electron mediators (cofactor) that are immobilized in contact with the active enzyme sites. Biomimetic dyes are used as electron mediators; they insert into the binding site on the enzyme and bind specifically and irreversibly without interfering with the catalytic activity of the enzyme. An illustration of the proof-of-concept microfluidic biofuel cell is shown in Fig. 1, with a schematic depiction of the surface-bound biocatalysts. The simple flat-plate microchannel design facilitates a high surface-to-volume ratio, effectively one-dimensional flow behavior, rapid cross-stream diffusion and straightforward surface preparation. Prior to assembly, an electrically conducting material is deposited on the interior surfaces to form the anode and cathode, and the enzymes are tethered directly to these layers.

The focus of this study is to model species transfer associated with heterogeneous chemical reactions and enzyme kinetics based on the microchannel geometry in Fig. 1. The first aim is to determine whether the process is diffusion limited or reaction rate limited. Secondly, various enzyme-electrode patterns coupled with coherent bulk velocities are investigated in order to realize efficient fuel cell operation. This is the first computational study of this technology, and the results are intended to provide guidelines for the design and fabrication of microfluidic biofuel cells exploiting consecutive reactions. The long-term objective is to integrate the forefront of molecular biology with advanced microfabrication techniques to produce practical biofuel cell systems with novel architectures that result in advanced functionality.

2. Method

2.1. Enzyme kinetics

An enzyme converts one chemical species (the substrate) into another one (the product). The substrate concentration distribution in the combined fuel and oxidant feed stream of a microfluidic biofuel cell depends on the rate of the heterogeneous chemical reactions taking place on the biocatalytic electrode surfaces. For now, we ignore the coupled effects of oxidant transport and cathode kinetics and instead focus on the anodic process. The Damköhler number represents the ratio of reaction velocity to diffusive velocity defined as

$$Da = \frac{k c_0^{\upsilon-1}}{D/L_c} \tag{1}$$

In this equation, k is a rate constant for heterogeneous reactions, c_0 the bulk concentration, υ the overall order of reaction, D the diffusion coefficient and L_c is a characteristic length. There are two common scenarios:

(1) $Da \gg 1$: diffusion limited scenario
The reaction rate is fast compared to substrate diffusion to the catalyst site. Substrate transport is occurring at its maximum rate with approximately zero concentration at the reaction surface.
(2) $Da \ll 1$: reaction rate limited scenario
Diffusion of species is fast compared to the reaction rate. The concentration of substrate at the reaction surface is approximately equal to the bulk concentration.

To determine if the biofuel cell is diffusion limited or reaction rate limited, an appropriate system to model is the well-known horse liver alcohol dehydrogenase (ADH) enzyme kinetics for ethanol oxidation to acetaldehyde. The ADH catalyzed reaction is a one-step process, namely

$$CH_3CH_2OH \xrightarrow{ADH} CH_3CHO + 2H^+ + 2e^-$$

Wild type horse liver ADH has a maximum turnover number for catalytic ethanol oxidation of $k_{cat}^{ADH} = 155\,s^{-1}$ for pH from 8 to 10 [17]. It is a dimer with an irregular shape which makes it difficult to measure its size. The unit cell of a $P2_1$ space group of a crystal structured form of ADH is reported to be $55.05 \times 73.63 \times 92.49$ Å ($\beta = 102.6°$) [18]. As a rule-of-thumb, its molecular cross-sectional area can be estimated to be around $A_c = 10^{-16}\,m^2$. If we assume that the electrode surface coverage of enzymes is complete, the maximum turnover rate for the

heterogeneous reaction can be calculated as

$$R_{\max} = k_{\text{cat}}[\text{E}] = \frac{k_{\text{cat}}}{A_{\text{c}} N_{\text{A}}} \tag{2}$$

The surface concentration of enzymes is in our case equal to $[\text{E}] = (A_{\text{c}} N_{\text{A}})^{-1}$. Thus, we get

$$R_{\max}^{\text{ADH}} = \frac{k_{\text{cat}}^{\text{ADH}}}{A_{\text{c}} N_{\text{A}}} = \frac{155}{10^{-16} \times 6.02 \times 10^{23}} = 2.6 \times 10^{-6} \text{mol m}^{-2}\,\text{s}^{-1}$$

The one-dimensional diffusive species flux is defined as

$$J = -D\frac{\partial c}{\partial x} \tag{3}$$

If we consider a microchannel $h = 20\,\mu\text{m}$ in height with a bulk ethanol concentration of 500 mM, the maximum diffusive flux of ethanol becomes

$$J = -D\frac{c_0}{h} \cong 10^{-9}\frac{0.5 \times 10^3}{20 \times 10^{-6}} = 2.5 \times 10^{-2}\,\text{mol m}^{-2}\,\text{s}^{-1}$$

Thus, species diffusion is about four orders of magnitude faster than the reaction rate, indicating that the system is reaction rate limited ($Da \ll 1$). Even if the turnover rate was improved by a factor of 100, the anodic process would still be reaction rate limited.

The methanol fuelled biofuel cell oxidizes methanol to carbon dioxide via the simplified three-step process

$$\text{CH}_3\text{OH} \xrightarrow{\text{MDH}} \text{HCHO} + 2\text{H}^+ + 2\text{e}^-$$

$$\text{HCHO} + \text{H}_2\text{O} \xrightarrow{\text{FalDH}} \text{HCOO}^- + 3\text{H}^+ + 2\text{e}^-$$

$$\text{HCOO}^- \xrightarrow{\text{FDH}} \text{CO}_2 + \text{H}^+ + 2\text{e}^-$$

The turnover numbers and average sizes of the three catalytic enzymes participating in this process are expected to be of the same order of magnitude as for ADH, and all systems are therefore expected to be reaction rate limited. These new enzymes appear less frequently in the literature and there is relatively little appropriate data. Table 1 presents a summary of the information available in enzyme databases. The relatively low MDH activity is strongly enhanced by a 50 kDa activator protein from the same organism, resulting in a 40-fold increase in the MDH turnover rate (included in the tabulated value) [20]. A protein purified from *Methylococcus capsulatus* has been shown to improve the specific activity of FalDH [23]. There are also higher specific activities available for FDH purified from *Pseudomonas oxalaticus* with cofactor methylene blue or NAD [24]. Turnover numbers are normally not available in the literature, but can be calculated based on the specific activity, v, as described by the Michaelis–Menten model for first-order, steady-state enzyme kinetics [25],

$$v = \frac{v_{\max} c_0}{K_{\text{m}} + c_0} \tag{4}$$

The sensitivity K_{m} is a measure of the changes in reaction velocity when the substrate availability is reduced, in fact, K_{m} represents the substrate concentration value at which the reaction velocity is half-maximum, $v = v_{\max}/2$. Catalytic oxidation of primary alcohols by alcohol dehydrogenases using cofactors in fact resembles two-substrate reactions described by the Theorell–Chance mechanism, where a ternary complex is presumably formed but its breakdown to yield the first product is very fast so that the ternary complex is kinetically insignificant [26]. With the cofactor bound to the enzyme, one can assume that the binding of substrate is the rate-limiting step as in an ordinary one-substrate mechanism, expressed in the classic Michaelis–Menten model of two-stage enzyme–substrate action,

$$\text{E} + \text{S} \underset{k_{-1}}{\overset{k_1}{\leftrightarrow}} \text{ES} \xrightarrow{k_2} \text{E} + \text{P}$$

The single substrate S binds reversibly to the enzyme E in the first stage, and the single product P is formed in the second stage. The sensitivity in Eq. (4) combines the effects of forward rate constant k_1, back rate constant k_{-1} and product formation rate constant k_2. Fig. 2 shows a typical Michaelis–Menten curve with normalized variables $v/v_{\max}$ and c_0/K_{m}. If the sensitivity is small relative to the bulk concentration, c_0, the specific activity is close to its maximum value. This implies that fuel cell

Table 1
Enzyme data valid for enzymes in solution

	MDH [20]	FalDH [21]	FDH [22]	ADH [17–19]
EC number	1.1.1.244	1.2.1.46	1.2.1.2	1.1.1.1
Organism	*B. methanolicus*	*P. putida*	*P. putida* sp. 101	*E. caballus*
Substrate	Methanol	Formaldehyde	Formate	Ethanol
Product	Formaldehyde	Formate	CO_2	Acetaldehyde
Cofactor	NAD	NAD	NAD	NAD
Number of subunits	10	4	6	2
Molecular weight (kDa)	430	250	280	–
Specific activity (μmol min^{-1} mg^{-1})	10.4	8.3	2.43	–
Max substrate conc. (M)	0.5	–	–	–
Required ions	Mg^{2+}, Zn^{2+}	–	–	–
Optimum temperature (°C)	–	30–40	40	–
Optimum pH	–	8.5	8	8–10
Sensitivity (mM)	0.99	0.2	0.62	7
Diameter (nm)	15			10

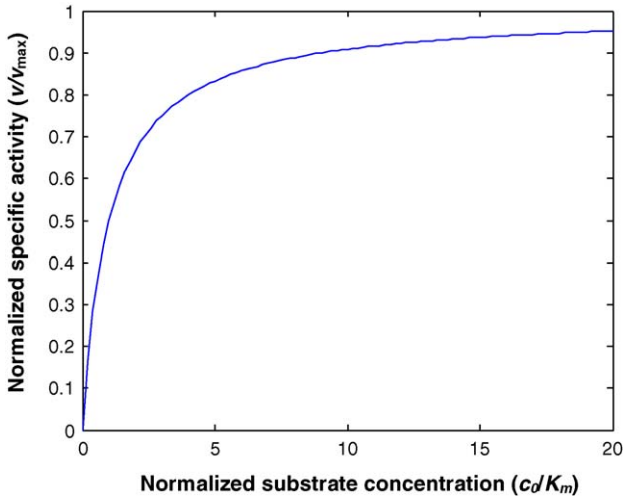

Fig. 2. Normalized Michaelis–Menten curve for enzyme kinetics.

operation near maximum specific activity is possible even with concentrations almost as low as K_m. For example if $c_0 = 5K_m$, we get $v = 0.83v_{max}$, which is only 17% short of the maximum value.

Specific activities found in the literature are often given in terms of catalytic turnover numbers per unit mass of protein in the enzyme sample. Assuming that the enzymes are fully purified, the actual molecular turnover number can be calculated as

$$k_{cat} = vM \tag{5}$$

The enzyme molecular mass, M, is also available in enzyme databases. Using Eq. (5) the maximum turnover numbers may be estimated as follows,

$$\text{MDH}: \quad k^{A}_{cat,max} = \frac{10.4 \times 10^{-6}}{60} \times 430 \times 10^{6} = 75\,s^{-1}$$

$$\text{FalDH}: \quad k^{B}_{cat,max} = \frac{8.3 \times 10^{-6}}{60} \times 250 \times 10^{6} = 35\,s^{-1}$$

$$\text{FDH}: \quad k^{C}_{cat,max} = \frac{2.43 \times 10^{-6}}{60} \times 280 \times 10^{6} = 11\,s^{-1}$$

We denote methanol, formaldehyde and formate oxidation with superscripts A, B and C, respectively. Note that the use of tabulated values for these calculations can be treacherous, as the values vary depending on variations in molecular structure and ambient conditions such as temperature and pH. Although these turnover numbers are expected to be order-of-magnitude correct, a targeted experimental study in this area would be very beneficial. To determine the flux of substrate and product to and from the electrode surface for a reaction rate limited system, we require estimates of the average size of the enzyme molecules and the average surface coverage. For an order-of-magnitude estimate we assume complete monolayer surface coverage and size equivalent to the cross-sectional area used for ADH, $A_c = 10^{-16}\,m^2$, for all three enzymes. The turnover rates are then

$$\text{MDH}: \quad R^{A}_{max} = \frac{75}{10^{-16} \times 6.02 \times 10^{23}} = 1.2 \times 10^{-6}\,mol\,m^{-2}\,s^{-1}$$

$$\text{FalDH}: \quad R^{B}_{max} = \frac{35}{10^{-16} \times 6.02 \times 10^{23}} = 5.7 \times 10^{-7}\,mol\,m^{-2}\,s^{-1}$$

$$\text{FDH}: \quad R^{C}_{max} = \frac{11}{10^{-16} \times 6.02 \times 10^{23}} = 1.9 \times 10^{-7}\,mol\,m^{-2}\,s^{-1}$$

If all the electrons released by the chemical reactions are captured by the electron mediators, the maximum current density at each enzyme patch is obtained by

$$i_{max} = zFR_{max} \tag{6}$$

Here, z represents the number of electrons released by oxidation of one substrate molecule. Note that all turnover parameters and current densities also depend on bulk concentration and enzyme sensitivity via the Michaelis–Menten model for first-order enzyme catalysis given in Eq. (4). The actual turnover rates and current densities are thus written as

$$R = R_{max}\frac{c_0}{K_m + c_0} \tag{7}$$

$$i = i_{max}\frac{c_0}{K_m + c_0} \tag{8}$$

As before, if the substrate concentration is high compared to the sensitivity ($c_0 \gg K_m$), the Michaelis–Menten kinetic effects can be neglected. This is not always the case in consecutive chemical processes, as some concentrations will approach zero, especially if effectively complete fuel utilization is achieved.

A complete biofuel cell must also contain a cathode, where the protons and electrons released at the anode are captured in order to provide a closed electrical circuit. The need for high pressures and temperatures make conventional O_2-reducing cathodes incompatible with biocatalytic anodes. For consistency with the specificity of the biofuel cell concept, the cathodic chemical reaction should also be catalyzed by suitable redox enzymes. Two options are considered in this work, either reduction of oxygen to water catalyzed by the bilirubin oxidase enzyme or peroxide reduction to water catalyzed by the catalase–peroxidase enzyme. Peroxide is preferable from an oxidant supply point-of-view given that it is miscible with water in all proportions and can easily be added to the liquid mixture in the microchannel. Oxygen for the cathodic reaction can also be dissolved in water, but only in relatively low concentrations. Alternatively, using a gas permeable backing material such as poly(dimethylsiloxane) (PDMS) [27], oxygen from the ambient air could diffuse through the backing layer to supplement the dissolved oxygen for the cathodic reaction. Oxygen has the advantage of being available in the ambient air whereas peroxide must be continuously supplied from a reservoir. The

overall cell potential is however limited by the potential difference between the anode and cathode redox couples, and it appears that the theoretical potential difference achievable with peroxide is somewhat higher than for oxygen. Moreover, the single enzyme cathodic reactions described here are expected to be faster than the anodic reactions [28,29]. The focus of this study is the biofuel cell anode, and its inherent kinetics are assumed to be independent of the cathode characteristics.

2.2. Species transport

The diffusion coefficient of small molecules in water at room temperature is normally around $D \approx 10^{-9}\ \mathrm{m^2\ s^{-1}}$, but increases exponentially with temperature. An enzymatic biofuel cell operating at its optimum temperature, say 40 °C, is likely to experience somewhat faster diffusion. Kulikovsky [30] recommends a reference value of $D_{\mathrm{ref}} = 1.58 \times 10^{-9}\ \mathrm{m^2\ s^{-1}}$ at $T_{\mathrm{ref}} = 298\ \mathrm{K}$ for methanol in water in void pores, and use the temperature dependence

$$D_{\mathrm{MeOH/H_2O}}(T) = D_{\mathrm{ref}}\ \exp(0.026236(T - T_{\mathrm{ref}})) \tag{9}$$

At optimum temperature (40 °C) we get $D = 2.34 \times 10^{-9}\ \mathrm{m^2\ s^{-1}}$. This value is assumed to be valid for all solutes.

Total species flux by diffusion and advection is described by

$$\vec{J} = -D\vec{\nabla}c + c\vec{u} \tag{10}$$

The ratio of advection to diffusion is defined by the Peclet number

$$Pe = \frac{L_{\mathrm{c}}\bar{u}}{D} \tag{11}$$

The average bulk velocity is denoted by $\bar{u}$, and L_{c} is a characteristic length. For high Peclet numbers, we may neglect diffusive flux at the inlet and outlet, and species transport becomes proportional to the local concentration. With this assumption, a useful analytical expression for the species concentration distribution may be derived. Taking heterogeneous chemical reactions into account and assuming maximum reaction rates, the species balance in a channel with rectangular cross-section can be written as

$$c_{\mathrm{in}}\bar{u}hw = \sum_j R^j_{\mathrm{max}} L^j w + c_{\mathrm{out}}\bar{u}hw \tag{12}$$

In this relationship, c_{in} is the inlet concentration, $\bar{u}$ the average velocity, h the channel height, w the channel width, L the length of each active enzyme patch and c_{out} the outlet concentration. For a single reaction process with only one type of enzyme fully covering the anode surface, the species balance at downstream position x in the microchannel becomes

$$c_{\mathrm{in}}\bar{u}h = R_{\mathrm{max}}x + c(x)\bar{u}h \tag{13}$$

Solving for the concentration, we get

$$c(x) = c_{\mathrm{in}} - \frac{R_{\mathrm{max}}}{\bar{u}h}x \tag{14}$$

This analytical result will be used to assess the accuracy of the numerical model.

The biofuel cell system is expected to exhibit low Damköhler numbers (reaction rate limited) and therefore essentially constant substrate concentration in the cross-stream direction. In order to get complete fuel utilization, we can then design the microchannel to match zero concentration at the outlet. But because of degrading enzyme kinetics it is rather inefficient to use concentrations close to zero. Moreover, the advective flux is reduced for near-zero concentrations and the diffusive part should again be added. Thus a 2D computational model incorporating diffusive flux and concentration dependent enzyme kinetics is required. Fuel utilization based on total flux for a single reaction process is calculated as

$$\mathrm{FU} = 1 - \frac{J_{\mathrm{out}}}{J_{\mathrm{in}}} \tag{15}$$

To determine overall fuel utilization for a consecutive process we need to include the other reaction steps as well. For methanol, two electrons are released in each step, so for complete fuel utilization we get six electrons per methanol molecule. Overall fuel utilization in terms of electrons doing actual work can therefore be defined as

$$\mathrm{FU} = 1 - \frac{6J^{\mathrm{A}}_{\mathrm{out}} + 4J^{\mathrm{B}}_{\mathrm{out}} + 2J^{\mathrm{C}}_{\mathrm{out}}}{6J^{\mathrm{A}}_{\mathrm{in}}} \tag{16}$$

For instance, 100% FU for the first step in a three-step process with 0% FU for the secondary steps would result in an overall FU of 33% using this equation.

In electrochemical devices, cross-stream transport may appear due to water involvement in the chemical reactions and electro-osmotic drag. But in microscale biofuel cells where diffusion is fast compared to reaction rates such effects do not intervene with substrate transport and may readily be neglected.

2.3. CFD model

A numerical model that solves the Navier–Stokes equations for the laminar velocity profile of the bulk flow and the convective diffusion equation for solute species transport is implemented in the commercially available software package FEMLAB 3.1. The 2D channel geometry under study is $h = 20\ \mu\mathrm{m}$ in height and $L = 30\ \mathrm{mm}$ long, which is considered fixed throughout the analysis. The continuum assumption is appropriate for liquid flows in microchannels of this scale, justifying the use of continuous flow theory and established computational fluid dynamics methods [31]. The Navier–Stokes equations for conservation of mass and momentum for steady incompressible flow are given as

$$\nabla \cdot \vec{u} = 0 \tag{17}$$

$$\rho\vec{g} - \nabla p + \mu\nabla^2\vec{u} = 0 \tag{18}$$

No-slip boundary conditions are applied at the channel walls with uniform inlet velocity $\bar{u}$ and constant outlet pressure. The flows modeled here exhibit low Reynolds numbers ($Re \approx 10^{-3}$), and are steady and fully developed over the majority of the computational domain. Gravity effects are neglected, and the flow is assumed to be isotropic and isothermal throughout the domain. The convective diffusion equation for solute species

conservation, with passive scalar treatment and the assumption of infinite dilution, is written as

$$\rho\frac{\partial c^i}{\partial t} + \rho\vec{u}\cdot\nabla c^i = \nabla(\rho D\nabla c^i) \quad (19)$$

c^i represents molar concentration of solute, and one separate convective diffusion equation is needed for each of the participating species. Source terms can readily be ignored since there are no homogeneous chemical reactions. Dirichlet boundary conditions are used at the inlet, that is, constant primary substrate concentration $c_{in} = 500\,\text{mM}$ representing a fuel reservoir and zero secondary species concentrations. Neumann boundary conditions are assigned to the cathode surface at $y = h$, describing an impermeable wall with zero concentration gradients $(\partial c^i/\partial y)|_{y=h} = 0$. At the anode surface at $y = 0$ we have concentration dependent flux due to the heterogeneous chemical reactions. Incorporating Michaelis–Menten kinetics for the enzyme catalyzed reactions, the boundary conditions can be written as $D(\partial c^i/\partial y)|_{y=0} = R^i_{max}(c^i/(K^i_m + c^i))$ for sinks and $D(\partial c^i/\partial y)|_{y=0} = -R^j_{max}(c^j/(K^j_m + c^j))$ for sources with $i \neq j$. Purely advective flux is applied for all solutes at the outlet, $(\partial c^i/\partial x)|_{x=L} = 0$.

The governing equations are coupled through velocity and chemical reactions, and can be solved either sequentially or simultaneously. The boundary conditions for the species conservation equations depend on concentration, which is one of the outputs of each iteration, and must be updated accordingly. For a consecutive process the anode boundary conditions may also depend on the concentration of other species. For example, the second species in a two-step process is produced at the same rate as the first species is consumed, i.e. its boundary condition at the production site will depend on the reaction kinetics of the first species. To solve all the governing equations of a consecutive system simultaneously thereby becomes very memory intensive. For improved efficiency, it is preferable to solve the equations sequentially as follows:

(1) Navier–Stokes equations $\rightarrow u, p$
(2) u, $c^A \rightarrow$ convective diffusion eq. for species A $\rightarrow c^A$ (iterate)
(3) u, c^A, $c^B \rightarrow$ convective diffusion eq. for species B $\rightarrow c^B$ (iterate)
(4) u, c^B, $c^C \rightarrow$ convective diffusion equation for species C $\rightarrow c^C$ (iterate)

These types of multiphysics problems are conveniently tackled using a finite element based methodology, which can handle a wide range of coupled non-linear physical problems with dependent boundary conditions. A direct solver type that converts the non-linear governing equations to linear systems is applied, using a non-iterative, fast and unconditionally stable (always converging) approach.

Mesh optimization is an important part of problem solving using CFD. Simple elongated unstructured triangular elements with manually refined sections are used for this study, mostly because of their flexibility. A thorough mesh convergence analysis was performed for simple one-step ethanol oxidation catalyzed by ADH enzymes. The substrate concentration was intentionally kept high such that Michaelis–Menten kinetics can be ignored. Mesh control was assessed by comparing numerical results to the analytical solution derived in Section 2.2. The selected mesh, including local mesh refinements in regions with high gradients, showed an accurate concentration profile as compared to the analytical result in Eq. (14) and was also computationally viable in the context of direct solver memory limitations.

3. Results and discussion

Maximum current densities obtained from Eq. (6) are $i^C_{max} = 4\,\mu\text{A cm}^{-2}$ for FDH, $i^B_{max} = 11\,\mu\text{A cm}^{-2}$ for FalDH and $i^A_{max} = 24\,\mu\text{A cm}^{-2}$ for MDH. Ethanol oxidation by ADH can reach a maximum current density of $i^{ADH}_{max} = 50\,\mu\text{A cm}^{-2}$, which is close to the value reported by Moore et al. [14], $53\,\mu\text{A cm}^{-2}$ for Nafion immobilized enzymes. However, Moore's group points out that their biofuel cell anode is mass transfer limited because of slow species transfer through the pore network of the Nafion structure, and does not fully utilize its feasible kinetics. With electron mediator cross-linking as in our case, enzymes exposed directly to the fuel facilitate much faster mass transfer and consequently higher current densities. Using enzyme kinetics data for enzymes in solution, as in this model, is therefore likely to underestimate reaction rates, and provide a conservative estimate of fuel cell performance.

Fig. 3 presents the concentration distribution in the channel for an ethanol fuelled ADH anode with the selected mesh, and also shows the extremely large aspect ratio of the geometry (1500:1). The inlet velocity is in this case tailored for 50% theoretical fuel utilization. The substrate concentration decreases linearly with axial length, with an outlet value of 254 mM, near the predicted 250 mM for ~50% fuel utilization. The discrepancy from the analytically predicted value appears when Michalis–Menten kinetics with relatively high sensitivity are introduced; marginally reducing the reaction rates even at high substrate concentrations. The average current density, determined by boundary integration, is approximately equal to i^{ADH}_{max}. As shown by the contours in Fig. 3, the substrate concentration

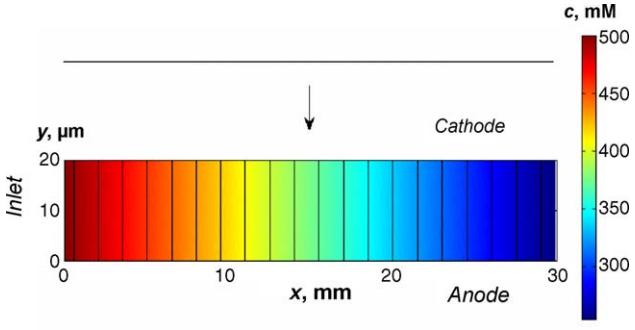

Fig. 3. Ethanol concentration in the microchannel with an ADH catalyzed anode at $y = 0$, plotted with magnified channel height. True channel geometry is shown above (aspect ratio 1500:1). Conditions: $c_{in} = 500\,\text{mM}$, $\bar{u} = 1.56 \times 10^{-5}\,\text{m s}^{-1}$, $h = 20 \times 10^{-6}\,\text{m}$, $L = 0.03\,\text{m}$.

is roughly constant in the cross-stream direction, indicating a reaction rate limited process.

To estimate the required pumping power for the microchannel flow, we calculate the pressure drop given from laminar flow theory [32] as

$$\Delta p = \frac{32\mu L\bar{u}}{D_h^2} \tag{20}$$

With hydraulic diameter $D_h = 2h$ the pressure drop becomes $\Delta p = 5.9$ Pa. The pumping power is equal to the pressure drop multiplied by the volumetric flow rate

$$\dot{W}_p = \dot{V}\Delta p = \bar{u}hw\Delta p \tag{21}$$

Furthermore, the overall power output of the fuel cell can be estimated as

$$\dot{W}_{out} = IV_{out} \cong iLwV_{out} \tag{22}$$

Per unit width, we get $\dot{W}_p/w \cong 10^{-9}$ W m^{-1} and $\dot{W}_{out}/w \cong 10^{-2}$ W m^{-1} ($V_{out} \cong 1$ V). The pumping power is thereby negligible.

A similar anode model is also established for three-step consecutive methanol oxidation to carbon dioxide. Six useful electrons are released in this process as opposed to only two for the one-step ethanol process. Considering the molecular mass of methanol and ethanol, respectively, the energy density of methanol is much higher. In fact, 4–5 times more useful electrons can be captured per unit mass of fuel. The methanol inlet concentration is set to 500 mM and the velocity is reduced relative to the ADH model because of additional steps and slower kinetics. As a starting point, the enzymes are distributed along the anode surface in three discrete, equally sized zones of 10 mm in length (case 1). The anode surface boundary is therefore divided into three parts and the turnover rates of MDH, FalDH and FDH are implemented in a stepwise fashion and assumed to be completely substrate specific. One electrical contact is required for each enzyme zone to avoid potential losses, and the zones have to be sufficiently separated to prevent leak currents. We assume this spacing to be thin compared to the zone lengths and apply the same microchannel geometry, material properties and other boundary conditions as in the ADH study. The solid lines of Fig. 4 present the resulting concentration distributions for a 50% methanol fuel utilization predictive inlet velocity. This figure effectively illustrates the reaction rate limited consecutive anodic process in a microchannel. The methanol concentration decreases linearly over the MDH enzyme zone, allowing the formaldehyde product concentration to increase at the same rate. Downstream of the MDH zone, the leftover methanol concentration remains constant. On the FalDH enzyme surface, formaldehyde is consumed to create formate on a one-to-one basis. The slope of the concentration curves is less steep, indicating slower kinetics than for MDH. Formate is slowly consumed on the FDH surface while the other concentrations are constant. Carbon dioxide formed on this surface is assumed to be dissolved or vented off in a way that does not disturb the kinetics of the FDH enzymes. The substrate concentrations at the outlet are $c_{out}^A = 277$ mM, $c_{out}^B = 104$ mM and $c_{out}^C = 80$ mM for

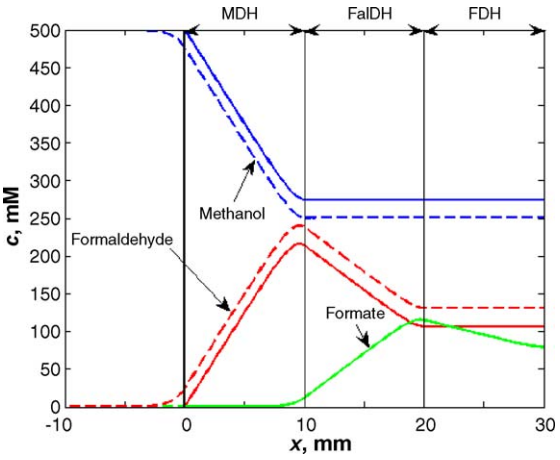

Fig. 4. Species concentration at the anode surface from inlet to outlet. Solid lines indicate results for an inlet at $x = 0$, whereas dashed lines correspond to results for an extended inlet section ($-0.01 < x < 0$ m). Conditions: $c_{in}^A = 500$ mM, $c_{in}^B = 0$ mM, $c_{in}^C = 0$ mM, $\bar{u} = 2.4 \times 10^{-6}$ m s^{-1}, $h = 20 \times 10^{-6}$ m. Enzyme patterning: $L^A = L^B = L^C = 0.01$ m (case 1).

the initial case without an extended inlet section (solid lines). The average current density is close to the maximum values for the individual enzymes, but ideally, the outlet concentrations should all be zero. Nonzero quantities indicate unused fuel and incomplete fuel utilization, which in this case is FU = 25%. The reason why c_{out}^A is much larger than the predicted 250 mM is that there is a significant diffusive flux (about 5%) entering the domain at the inlet. To isolate this effect, an extended 1 cm long non-catalyzed section is added to the inlet region in the numerical model. Results with an extended inlet region are shown as dashed lines in Fig. 4 and compared to the previous results. The outlet concentrations are now $c_{out}^A = 252$ mM, $c_{out}^B = 128$ mM and $c_{out}^C = 80$ mM with overall fuel utilization FU = 27%. The main difference is that all species are allowed to diffuse across the interior boundary at $x = 0$, even though the methanol flux entering the domain at $x = -0.001$ m is purely advective. In reality, the fuel reservoir and electrodes ought to be separated

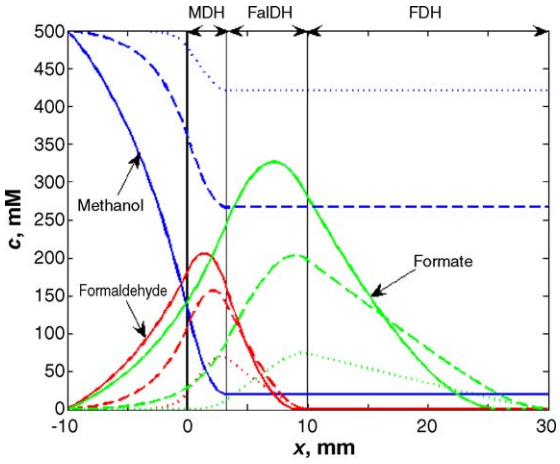

Fig. 5. Species concentration at the anode surface from inlet to outlet for various average velocities ($\bar{u} = 2.4 \times 10^{-6}$ m s^{-1} for dotted lines, $\bar{u} = 0.8 \times 10^{-6}$ m s^{-1} for dashed lines and $\bar{u} = 0.3 \times 10^{-6}$ m s^{-1} for solid lines). Enzyme patterning: $L^A = 3.2$ mm, $L^B = 6.7$ mm, $L^C = 20.1$ mm (case 2).

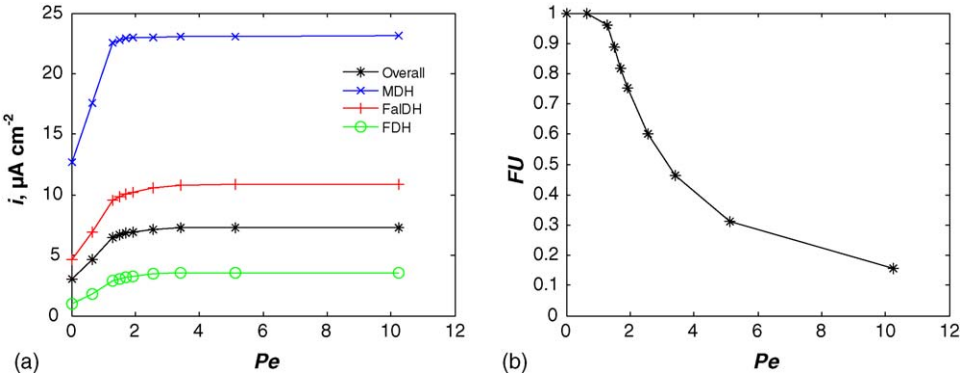

Fig. 6. Current densities (a) and fuel utilization (b) vs. Peclet number. Enzyme patterning: $L^A = 3.2$ mm, $L^B = 6.7$ mm, $L^C = 20.1$ mm (case 2).

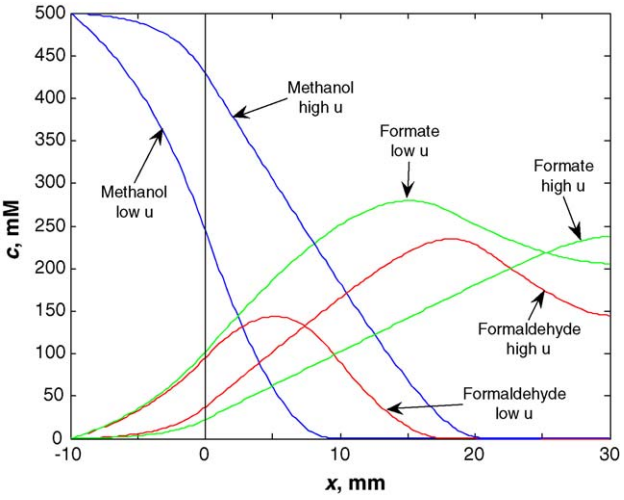

Fig. 7. Concentration distributions at the anode surface for two bulk velocities; high ($\bar{u} = 8 \times 10^{-7}$ m s^{-1}) and low ($\bar{u} = 3 \times 10^{-7}$ m s^{-1}). Enzyme patterning: mixed 1:1:1 (case 3).

in this manner by some inlet feed section with no chemical reactions.

In order to improve fuel utilization, we have to take advantage of the difference in turnover rates for the various enzymes. The zones with low turnover rates should be extended at the expense of the high rate zones. Since each reaction generates an equivalent number of electrons, the optimal lengths of the zones correspond to the ratio $1/R^A{:}1/R^B{:}1/R^C$. Assuming that $R = R_{max}$ everywhere, we get

$$L^i = \frac{(R^i_{max})^{-1}}{\sum_j (R^j_{max})^{-1}} L, \quad i = \mathrm{A, B, C}, \quad j = \mathrm{A, B, C} \tag{23}$$

For the three-step methanol process, the optimal lengths become $L^A = 3.2$ mm, $L^B = 6.7$ mm and $L^C = 20.1$ mm, which are applied in case 2. Fig. 5 shows concentration profiles with respect to these zone lengths, obtained for three different bulk velocities. Again, an extended inlet section is used. For the same velocity as in case 1 (dotted lines), the methanol concentration remains high and the other concentrations are low throughout. Case 1 does actually perform better than case 2 at high velocities. In order to reach high fuel utilization the velocity must be reduced, as can be seen by the improved methanol concentration drop as the velocity is cut down. Simultaneously, as we reduce the velocity, *Pe* numbers approach unity and an increased fraction of diffusive flux enters the non-catalyzed inlet section. An important issue to note in the case of low *Pe* is that the secondary species are able to diffuse back into the inlet section. For the lowest velocity ($\bar{u} = 0.3 \times 10^{-6}$ m s^{-1}), both formaldehyde and formate are able to diffuse back all the way to the fuel reservoir. Back diffusion of secondary species will in principle have no effect on fuel utilization, but it can reduce current densities due

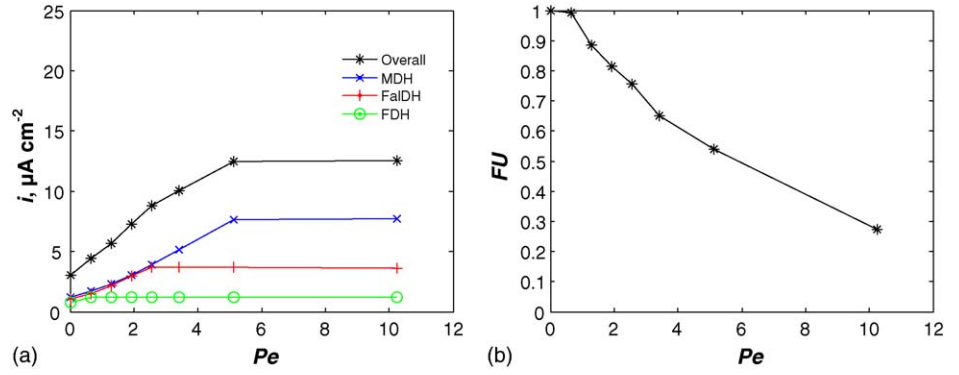

Fig. 8. Current densities (a) and fuel utilization (b) vs. Peclet number. Enzyme patterning: mixed 1:1:1 (case 3).

to a lack of secondary fuel at the enzyme sites. Current densities at the individual enzyme zones as well as the overall current density are shown in Fig. 6a, where the Peclet numbers are based on the characteristic length scale for streamwise diffusion, $L_c = 0.01$ m. The current densities decrease rapidly as the rate of diffusion overrides the rate of advection ($Pe < 1$). On the other hand, all current densities are remarkably stable in the advection dominated regime. Fuel utilization is near 100% in the diffusion dominated and mixed regimes, as indicated in Fig. 6b, unaffected by back diffusion. It is also shown that the enzyme turnover rates cannot keep up with the species transport as the velocity reaches some threshold value, causing less fuel efficient operation with unused fuel at the outlet.

Another option for the anode enzyme patterning is to mix all three types throughout the entire electrode surface using only one electrical contact, which is preferable from a fabrication point-of-view. The simplest option is to mix the enzymes on a 1:1:1 molecular basis, denoted by case 3, such that each enzyme covers one third of the surface area and the turnover rates become

$$R = \frac{1}{3} R_{\max} \frac{c}{K_m + c} \tag{24}$$

Concentration profiles for case 3 are presented in Fig. 7 for two different bulk velocities. In general, the concentration distributions are similar to the results of case 1, where a large flux of secondary species is leaving the domain at the outlet. To measure this effect, current densities (a) and overall fuel utilization (b) are given in Fig. 8 as functions of the Peclet number. High current densities are obtained in the advection dominated regime but the fuel utilization for high *Pe* is poor. The fuel efficiency is only sufficient in the diffusion dominated regime. It is therefore difficult to find an appropriate balance between these two parameters for the mixed enzyme electrode design, unless the individual enzyme surface coverage ratios are modified. Matching the surface coverage to the turnover rates, as in case 2, we utilize the ratios $1/R^A{:}1/R^B{:}1/R^C$. The new turnover rates adopted in case 4 are calculated by

$$R = \frac{(R_{\max})^{-1}}{\sum_j (R^j_{\max})^{-1}} R_{\max} \frac{c}{K_m + c}, \qquad j = \mathrm{A, B, C} \tag{25}$$

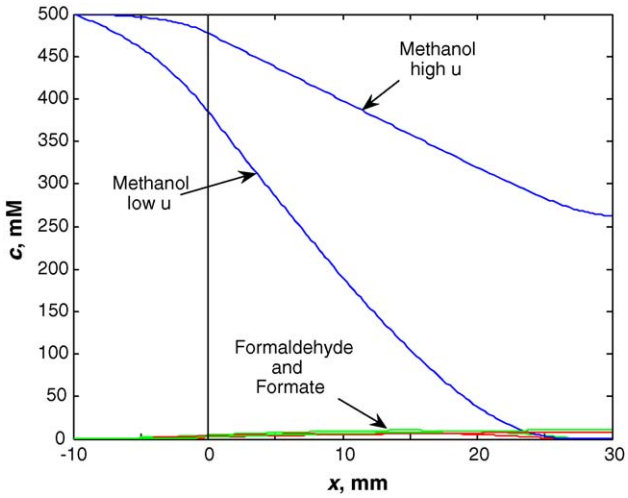

Fig. 9. Concentration distributions at the anode surface for two bulk velocities; high ($\bar{u} = 8 \times 10^{-7}$ m s^{-1}) and low ($\bar{u} = 3 \times 10^{-7}$ m s^{-1}). Enzyme patterning: mixed $1/R^A{:}1/R^B{:}1/R^C$ (case 4).

The concentration profiles obtained for case 4 are shown in Fig. 9 for the same velocities as in Fig. 7. The rate of methanol consumption is slower than in case 3 as the MDH fraction is reduced, but significant improvements are attained in terms of secondary species outlet concentrations. Fig. 10 presents current densities and fuel utilization for case 4. In this case, fuel utilization remains high and steady for a wider range of Peclet numbers. Maximum current densities are lower than for case 3 but can be realized for most *Pe* above unity. It is possible to combine high current densities with high fuel usage for this enzyme patterning strategy. For example, $Pe = 1.5$ provides 7.0 μA cm^{-2}, which is 99% of the maximum current density for case 4, at 99% fuel utilization.

To summarize the results obtained for the anodic three-step methanol oxidation process, Fig. 11 presents a comparison of current densities and fuel utilization for cases 1–4 at low Peclet numbers. The diffusion dominated regime ($Pe < 1$) is not recommended due to low current densities. Fuel cell performance is generally better in the mixed regime ($1 < Pe < 2$) where reasonably high current densities are met by nearly complete fuel utilization, with case 4 showing superior characteristics. In the

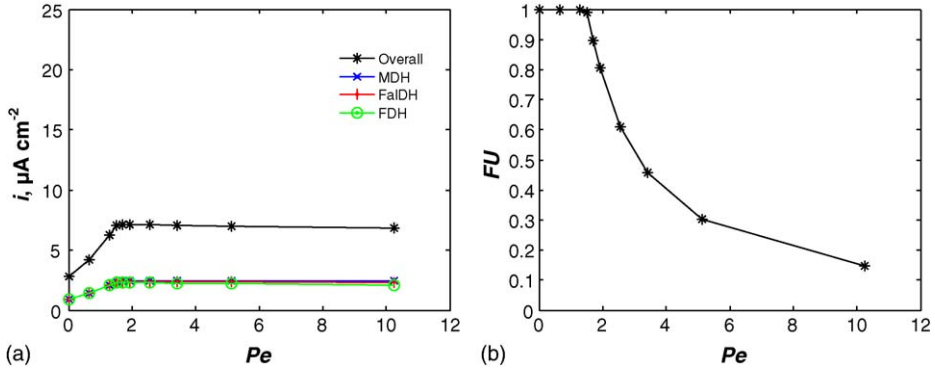

Fig. 10. Current densities (a) and fuel utilization (b) vs. Peclet number. Enzyme patterning: mixed $1/R^A{:}1/R^B{:}1/R^C$ (case 4).

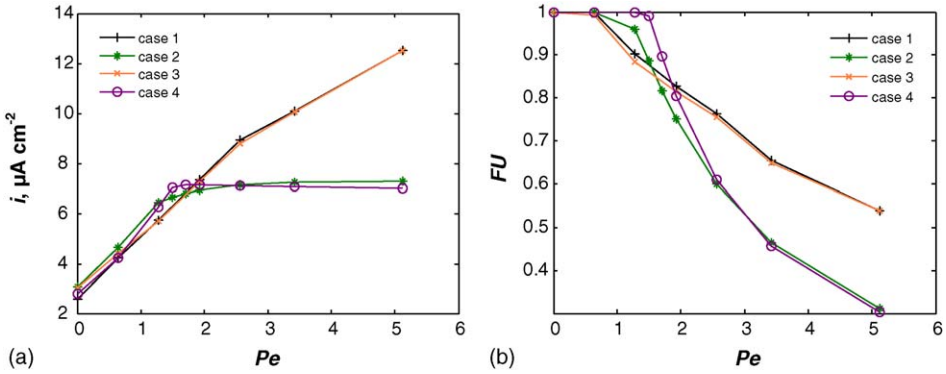

Fig. 11. Current density (a) and fuel utilization (b) comparison for enzyme arrangements according to cases 1–4.

advection dominated regime, cases 1 and 3 are the preferable choices although fuel utilization is poor.

4. Conclusions

A microstructured enzymatic biofuel cell architecture for consecutive chemical reactions was proposed, and species transport coupled with laminar flow and Michaelis–Menten kinetics was studied in 2D using a numerical approach. Biofuel cell performance was shown to be limited by the reaction rates associated with enzyme kinetics. Turnover rates for individual enzymes were key parameters throughout this analysis and directly determined the realizable current densities. The pumping power required for the microchannel flow was determined to be negligible compared to the predicted output power of the unit cell.

The current densities obtained for one-step enzyme catalyzed ethanol oxidation were generally higher than for consecutive methanol oxidation. If maximum current density is the only target, one-step ethanol oxidation is thereby recommended. Methanol is, however, the more attractive fuel in terms of energy density, as 4–5 times more electrons can be captured per unit mass of fuel. Four separated and mixed electrode enzyme patterning strategies were presented, and tested with various bulk velocities to optimize overall current density and fuel utilization. Nearly complete fuel utilization was accomplished in the diffusion dominated and mixed species transport regimes. Local current densities are high and steady in the advection dominated regime, but become significantly reduced for low velocities because of back diffusion and fuel supply shortcomings. The mixed transport regime is therefore particularly attractive for biofuel cell operation, with particularly superior characteristics shown for mixed enzyme patterning that accounts for individual turnover rates. Overall current density is mainly limited by the slow turnover rates for formate and formaldehyde oxidation by FalDH and FDH. Finding new or modified enzymes with higher turnover numbers is a sound strategy to improve the performance of this technology. Inclusion of proper enzyme–electrode tethering is expected to enhance current densities, and accurate measurements of individual turnover numbers for tethered enzymes are desired for further advancements.

Acknowledgements

The funding for this research provided by a Natural Sciences and Engineering Research Council (NSERC) strategic grant and by Angstrom Power Inc. is highly appreciated. The authors also thank Dr. Ned Djilali for helpful comments.

References

[1] J. Larminie, A. Dicks, Fuel Cell Systems Explained, 2nd ed., John Wiley & Sons Ltd., Chichester, England, 2003.
[2] C.K. Dyer, J. Power Sources 106 (2002) 31–34.
[3] E. Kjeang, J. Goldak, M.R. Golriz, J. Gu, D. James, K. Kordesch, Fuel Cells, in press.
[4] S. Wasmus, A. Küver, J. Electroanal. Chem. 461 (1999) 14–31.
[5] E. Kjeang, J. Goldak, M.R. Golriz, J. Gu, D. James, K. Kordesch, J. Power Sources 153 (2006) 89–99.
[6] H.P. Bennetto, Biotechnol. Educ. 1 (4) (1990) 163–168.
[7] D.H. Park, J.G. Zeikus, Appl. Environ. Microbiol. 66 (4) (2000) 1292–1297.
[8] E. Katz, A.N. Shipway, I. Willner, in: W. Vielstich, H.A. Gasteiger, A. Lamm (Eds.), Biochemical Fuel Cells, Handbook of Fuel Cells—Fundamentals, Technology and Applications, vol. 1, John Wiley & Sons, Ltd., New York, 2003.
[9] A. Bazylak, D. Sinton, N. Djilali, J. Power Sources 143 (1–2) (2005) 57–66.
[10] S. Litster, D. Sinton, N. Djilali, J. Power Sources 154 (2006) 95–105.
[11] C. Ma, L. Zhang, S. Mukerjee, D. Ofer, B. Nair, J. Membr. Sci. 219 (1–2) (2003) 123–136.
[12] R.H. Borgwardt, Transport. Res. Part D 6 (2001) 199–207.
[13] S.C. Barton, J. Gallaway, P. Atanassov, Chem. Rev. 104 (2004) 4867–4886.
[14] C.M. Moore, S.D. Minteer, R.S. Martin, Lab on a Chip 5 (2005) 218–225.
[15] I. Willner, E. Katz, Angew. Chem. Int. Ed. 39 (2000) 1180–1218.
[16] C.M. Moore, N.L. Akers, S.D. Minteer, Proceedings of the 204th Meeting of The Electrochemical Society, 2003 (Abs. 1225).
[17] L.A. LeBrun, D.H. Park, S. Ramaswamy, B.V. Plapp, Biochemistry 43 (11) (2004) 3014–3026.
[18] H.W. Adolph, P. Zwart, R. Meijers, E.S. Cedergren-Zeppezauer, Annual Report 1998. EMBL Hamburg Outstation at Deutsches Elektronensynchrotron DESY, Hamburg, 1999, pp. 345–346.
[19] R. Pietruszko, Meth. Enzymol. 89 (1982) 429–435.
[20] H.J. Hektor, H. Kloosterman, L. Dijkhuizen, J. Biol. Chem. 277 (49) (2002) 46966–46973.
[21] W. Hohnloser, B. Osswald, F. Lingens, Hoppe Seylers Z. Physiol. Chem. 361 (12) (1980) 1763–1766.

[22] V.V. Karzanov, Y.A. Bogatsky, V.I. Tishkov, A.M. Egorov, FEMS Microbiol. Lett. 60 (1989) 197–200.
[23] S. Tate, H. Dalton, Microbiology 145 (1999) 159–167.
[24] T. Hopner, U. Ruschig, U. Muller, P. Willnow, Meth. Enzymol. 89 (1982) 531–537, Pt D.
[25] R.A. Copeland, Enzymes: A Practical Introduction to Structure, Mechanism and Data Analysis, 2nd ed., Wiley-VCH Inc., New York, 2000.
[26] N.C. Price, L. Stevens, Fundamentals of Enzymology: The Cell and Molecular Biology of Catalytic Proteins, 3rd ed., Oxford University Press Inc., New York, 1999.
[27] J.C. McDonald, D.C. Duffy, J.R. Anderson, D.T. Chiu, H. Wu, O.J.A. Schueller, G.M. Whitesides, Electrophoresis 21 (2000) 27–40.
[28] K. Johnsson, W.A. Froland, P.G. Schultz, J. Biol. Chem. 272 (5) (1997) 2834–2840.
[29] J.P. Chen, H.Y. Wang, Biotechnol. Tech. 12 (1998) 851–853.
[30] A.A. Kulikovsky, J. Appl. Electrochem. 30 (2000) 1005–1014.
[31] N.T. Nguyen, S.T. Wereley, Fundamentals and Applications of Microfluidics, Artech House, Boston, MA, 2002.
[32] C.T. Crowe, D.F. Elger, J.A. Roberson, Engineering Fluid Mechanics, 7th ed., John Wiley & Sons Inc., New York, 2001.